Thin Solid Films 591 (2015) 363–367

Contents lists available at ScienceDirect

Thin Solid Films

journal homepage: www.elsevier.com/locate/tsf

# Investigation of the role of vacancy sources and sinks on the Kirkendall-effect on the nanoscale

J. Tomán, C. Cserháti *, Y. Iguchi, Zs. Jánosfalvi, Z. Erdélyi

*Department of Solid State Physics, University of Debrecen, P. O. Box. 2, H-4010 Debrecen, Hungary*

ARTICLE INFO

Available online 8 May 2015

*Keywords:*
Kirkendall effect
Diffusion
Nanoscale
Vacancy sources and sinks

ABSTRACT

It is well-known that Kirkendall shift occurs in binary systems. We investigated diffusion on the nanometer scale in the framework of our conceptual model [Erdélyi and Schmitz, Acta. Mater. 60 (2012) 1807]. Since on this lengthscale the characteristic distances between the vacancy sources/sinks can be comparable to the dimensions of the sample, the usual vacancy annihilation processes, leading to the Kirkendall shift, cannot operate. In this situation, we studied the Kirkendall shift in planar geometry in case of miscible and restrictedly miscible systems by computer simulation.



## 1. Introduction

Since its discovery in 1947, the Kirkendall effect has played an important role in the development of solid state diffusion theory. Ernest Kirkendall in his third and last paper in a series [1–3] on the diffusion of Zn in $\alpha$-brass presented the results of his diffusion couple experiment. He electroplated a brass-bar with pure copper, but before that he placed inert Mo-wires along each of the two surfaces to mark the original interfaces of the diffusion couple. After heat treatments of different times cross sections of the diffusion couple were investigated and Kirkendall found that the wires shifted inwards moving parabolically with the annealing time. He explained this observation with that the Zn-atoms move much faster outwards than the Cu-atoms inwards, causing the inner brass to shrink. The first theoretical description was made by Darken [4] using independent diffusion fluxes for the different constituents. Based on these results, Seitz [5] and Bardeen [6] showed from atomistic point of view, that the interdiffusion accompanied by vacancy mechanism lead to Darken's equations if it is assumed that the vacancy concentration is in local equilibrium. Vacancies should be created on one side and annihilated on the other side of the diffusion couple for the Kirkendall effect to occur.

The manifestation of the Kirkendall effect, besides the marker movement, can be the appearance of diffusional porosity (Kirkendall voids [7,8]), generation of stresses [8,9] and the deformation of the whole specimen on the macroscopic scale [10]. Hollow nanoshell and nanowire formation was also explained by the Kirkendall effect [11–13].

In this study we are presenting a finite volume method to describe the interdiffusion process, as well as the Kirkendall effect on the nanoscale.

* Corresponding author.
*E-mail address:* cserhati.csaba@science.unideb.hu (C. Cserháti).

## 2. Diffusion fundamentals

As it is clear from Kirkendall's work, the effect can be best visualized by the motion of inert markers placed along the diffusion zone. The intrinsic diffusion fluxes of the components $j_i$[mol/m$^2$s], which reflect the mobilities of the different species involved in the interaction, are then defined with respect to this array of markers, called the Kirkendall frame of reference:

$$j_i = -D_i \frac{\partial C_i}{\partial x}. \tag{1}$$

Here $D_i$[m$^2$/s] is the intrinsic diffusion coefficient, $C_i$[mol/m$^3$] is the concentration of component $i$ and $x$[m] is the position parameter. In case of an A–B binary diffusion couple the equations for the intrinsic fluxes are:

$$j_A = -D_A \frac{V_B}{V_m^2} \frac{\partial N_A}{\partial x}, \quad j_B = -D_B \frac{V_A}{V_m^2} \frac{\partial N_B}{\partial x}, \tag{2}$$

where $N_i$ is the mole fraction of species A or B, $V_m$ [m$^3$/mol] is the molar volume, $V_i$ [m$^3$/mol] are the partial molar volumes of the different atoms [14,15]. The latter is found through the tangent construction in the $V_m$ vs. $N_i$ plot [16].

In writing Eq. (1) we followed the traditional Fick's approach, where the atomic flux is related to the gradient of the concentration (in moles per unit volume). There are of course more advanced methods using the Onsager flux expressions for the intrinsic atomic fluxes that involve transport coefficients and thermodynamic forces acting on the atomic species. In this case the gradient of concentration is replaced with the corresponding gradient of mole fraction as required by the expression for the thermodynamic forces [17,18,27].

http://dx.doi.org/10.1016/j.tsf.2015.04.089
0040-6090/

The marker velocity depends on the difference in intrinsic diffusivities of the species and the concentration gradient developing in the diffusion zone at the marker plane composition [4]:

$$v = -(V_B j_B + V_A j_A) = -V_B(D_A - D_B)\frac{\partial C_B}{\partial x}. \quad (3)$$

In these calculations it is always supposed that only a volume diffusion controlled process operates. If this is the case, the inert markers positioned at the original interface between the reactants are the only markers that stay at a constant composition and move parabolically in time ($x^2 \propto t$ or $x \propto t^{1/2}$) during the whole interdiffusion process. The velocity of these markers is:

$$v_K = \frac{dx}{dt} = \frac{x_K}{2t}, \quad (4)$$

where $x_K$ is the position of the Kirkendall plane. The location of the Kirkendall plane in the diffusion zone can be found graphically as the intersection between the marker velocity plot $2tv$ vs. $x$ and the straight line $2tv_K = x_K$ given by Eq. (4). In order to draw the line $2tv_K = x_K$, one needs to know the position of the plane in the diffusion zone where the inert markers were located at the beginning of the diffusion process, i.e. at time $t = 0$. However, if the total volume of the specimen does not change during the interdiffusion, this position can be determined by the usual Boltzmann–Matano method [14,15]. This kind of measurement allows us to determine the intrinsic diffusion coefficients at a single composition, namely that of the Kirkendall marker plane. To extend the measurement over the entire concentration range, a so-called multifoil diffusion technique has been introduced [19,20]. The characteristic feature of such a sample is, that each end-member of the diffusion couple is composed of several thin foils with fiducial markers in between. Interdiffusion in such a multilayered sample will cause the markers to move relative to the laboratory-fixed frame of reference. In the particular case of [20], 20 μm Pd and 21 μm thick Ni foils were used with $ThO_2$ powder as fiducial markers (the diameter of the oxide particles was ~0.5–1 μm). By measuring the shift of the markers, the Kirkendall displacement was determined over the entire concentration range and the displacement curve was constructed. Cornet [21,22] and later van Loo [23] proposed a method to obtain the Kirkendall velocity and then the intrinsic diffusion coefficient from the displacement curve. It was found to be:

$$v = \frac{1}{2t}\left(y - x_o\frac{dy}{dx_o}\right), \quad (5)$$

with $x_o$ being the original location of the markers at $t = 0$, $y$ is the displacement of the markers, i.e. $y = x - x_o$ and $t$ is the annealing time. As it is clear from Eq. (5), the position of the Kirkendall plane, as marked by inert markers placed at the initial interface ($x_o = 0$), is given by $v_K = y/2t$ ($v_K$ is the velocity of the markers placed at the initial contact interface). This also means that the Kirkendall plane can be found graphically as the intersection between the marker velocity plot (Eq. (5)) and the straight line ($2tv_K = x_K$), supposing that at $t = 0$ time the markers were at $x_o = 0$.

In this study we are modeling the above described phenomenon. Based on our conceptual model [24], a one dimensional finite volume method was developed. The planar sample was divided into $n$ slabs ($n = 2000$), where each slab mimics a metallic foil in the above described multifoil experiment. Note, that the number of the slabs only influences the spatial resolution of the calculated concentration profiles. In each computational cycle the total number of atoms transported between the neighboring slabs was calculated from which the change of composition as well as the thickness of the slab were determined. During the calculations the walls of the slabs are taken as markers in a multifoil experiment. From the calculations we get the displacement curve by registering the positions of the cell walls and the number of computation cycles. The velocity curve was calculated from Eq. (5) as a usual procedure in case of multifoil experiments.

For the computer simulation a simplified version of the model described in [24] was implemented. In that work a complete set of analytical equations was developed in order to describe reactive diffusion in spherical core shell nanostructures. The model takes into account elastic stress, its plastic relaxation, as well as possible non-equilibrium vacancy densities. Furthermore, thermodynamic driving forces are included to model formation of intermetallic product phases in intermediate composition range. Here we use the planar version of these equations (see the Appendix A. in [24]). In addition the effect and the change of the molar volume during the interdiffusion as well as the consequences of the developing stresses were neglected. On the other hand, considering that the vacancy concentration changes due to the atomic fluxes as well as due to the activity of vacancy sinks and sources, the continuity equation written in the Kirkendall reference system contains the vacancy flux and the term of vacancy sources and sinks as well. Including these terms into Fick's second law we arrive at:

$$\frac{\partial N_i}{\partial t} = -V_m(\nabla j_i x + N_i S_v), \quad (6)$$

where $S_v[\mathrm{mol}\cdot\mathrm{m}^{-3}\cdot\mathrm{s}^{-1}]$ is the vacancy source term, i.e. the number of vacancies created in unit volume per unit time. This expression is very similar to [17,18]. We define $s_v$ as:

$$s_v = S_v \cdot V_m = K_r\left(C_v^o - C_v\right), \quad (7)$$

which is the rate of change of the atomic fraction of vacancies due to creation/annihilation. $K_r$[1/s] determines the effectiveness of sinks and sources, therefore $s_v$ is proportional to the deviation of the vacancy concentration from it's equilibrium value. Note that $K_r$ may vary with spatial coordinates, depending on the spatial distribution of the sinks and sources. Since $K_r$ is a function of space, the solution of the diffusion equation, i.e. the movement of the inert markers will not follow the so called parabolic law (Note that taking constant $K_r$ the solution adheres to the traditional parabolic time evolution.). Another effect which may alter the parabolic behavior of the diffusion process is the finite size of the sample. When the diffusion profile reaches the end of the diffusion couple, the kinetic of the process is changing.

## 3. Results of the computer simulation

The algorithm and the selection of the input parameters were similar to the ones presented in [24]. Several cases have been studied. In order to validate our calculations we performed simulations using the parameters given in [20,25]. The intrinsic diffusivities were concentration dependent, but the ratio of the diffusivities was constant ($D_A / D_B =$ const.). The interdiffusion coefficient ($\tilde{D} = C_B V_B D_A + C_A V_A D_B$) was also constant in the whole concentration range. Studies have been completed in ideal solid solutions with vacancy sinks and sources active enough in every cell of the one dimensional finite volume model to maintain equilibrium vacancy concentration during the whole process. Fig. 1 displays a representative plot showing that our model safely reproduces the calculations, implemented in the traditional Darken's model [25], as well as the experimental observations reported in [25]. The scale on the horizontal and vertical axes is in arbitrary units on the figures. The dashed and the solid lines mark the displacement and the velocity curve respectively. The straight line represents the ($2tv_K = x_K$) equation. The interdiffusion coefficients published in [20] were used to calculate the concentration profiles and the corresponding Kirkendall displacement and velocity curves. It can be clearly seen, that the displacement as well as the velocity curves are almost exactly follow the trace of the experimental data presented

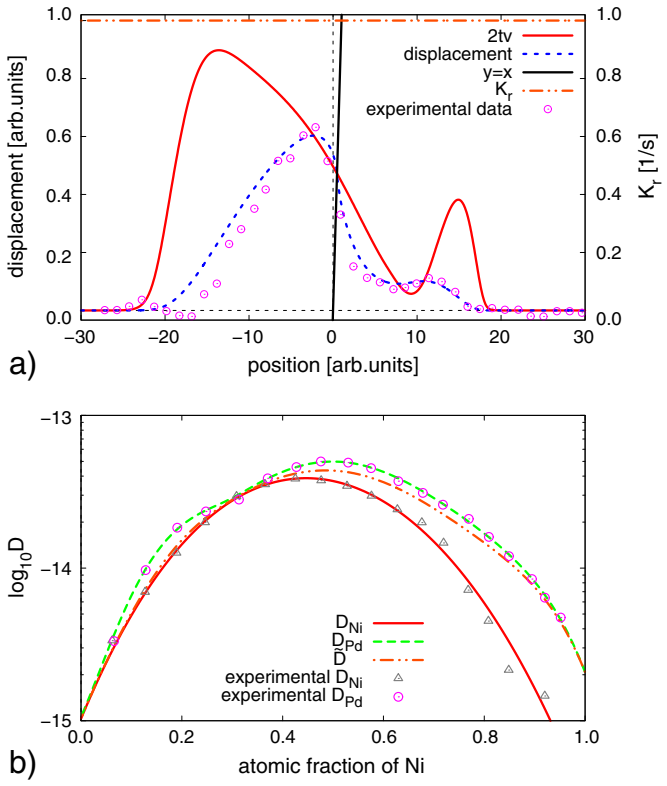


**Fig. 1.** Representative plot, showing the validity of our model. The displacement (dashed line) and the velocity curve (solid red line) on plot (a) are the same as in Figs. 10 and 14 in [20]. Plot (b) shows the concentration dependence of the interdiffusion coefficient, as well as the intrinsic diffusivities of the different species. The experimental data-points are replotted from [20].

(displacement curve) on Fig. 10 and the velocity curve on Fig. 14 in [20]. Fig. 1b demonstrates the composition dependence of the diffusivities. Note the logarithmic scale on the vertical axis.

We extended our studies to immiscible systems too and also by changing the arrangement of vacancy sources and sinks along the sample. Concentration dependent diffusivities have been used with various composition dependence.

We simulated the diffusion process in which the diffusivities depend exponentially on the concentration (for instance $D_i = D_{io}exp(mN_i)$, where $i = A$ or $B$), moreover the ratio of the diffusivities is constant. Fig. 2a shows the displacement (dashed line) as well as the velocity curve (solid red line) when the vacancy sources and sinks are evenly active in every slab (foil). On Fig. 2b the same is plotted but with a different vacancy source and sink distribution. As it was mentioned before, $K_r$ in Eq. (7) may vary along the sample. It was supposed that the vacancy sources and sinks are active enough in the slabs in the very vicinity of the starting interface to maintain the equilibrium vacancy concentration all the time ($K_r = 1/s$) but beyond that their activities approach to zero following a Gaussian distribution. For the sake of simplicity we will call this distribution of vacancy sinks and sources Gaussian in this paper (see the dot-dashed curve on Fig. 2b). This is a practical assumption since there are always impurities at the contact plane. Fig. 2c demonstrates the composition dependence of the diffusivities. Note the logarithmic scale on the vertical axis.

As it was expected based on the consideration of Philibert [15], the maximum of the velocity curve and that of the displacement curve coincide with the position of the Kirkendall plane for the case of constant ratio of intrinsic diffusivities in both cases. On the other hand, the velocity curve in Fig. 2b shows a local maximum at the Kirkendall plane (which in this case coincides with the Matano plane), the global maximum is more to the left. This means that although the Kirkendall plane is stable, the markers placed on positions where the gradient of the velocity curve is negative (left to the Kirkendall plane) get closer to each other during the process, which means another condensation of the markers, which is different from the Kirkendall plane. In case of a system having a miscibility gap similar results were obtained. The maximum of the velocity curve and displacement curve in this case also coincides with the position of the Kirkendall plane and altering the distribution of the sources and sinks to a Gaussian one, the velocity curve changes considerably, showing another local maximum, indicating similar behavior as in ideal solid solution.

Fig. 3a shows again the displacement as well as the velocity curve when the vacancy sources and sinks are evenly active in every slab

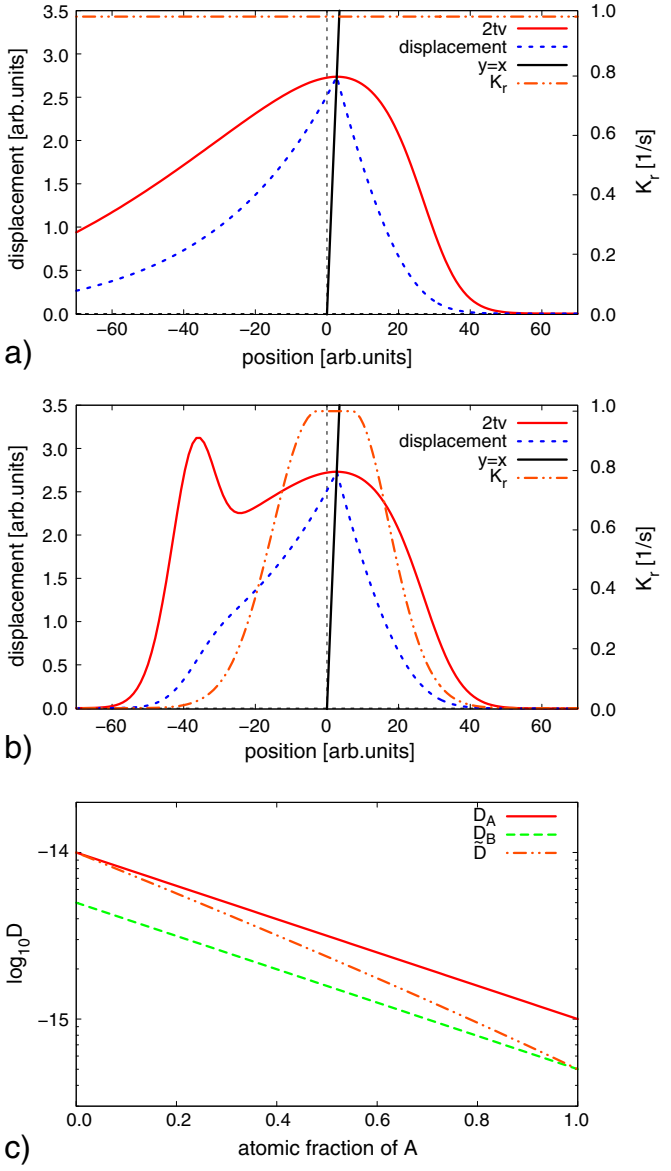


**Fig. 2.** In case of ideal solid solution plot (a) shows the displacement (dashed line) as well as the velocity curve (solid red line) when the vacancy sources and sinks are evenly active at every slab. On plot (b) the same is presented but with a Gaussian vacancy source and sink distribution (dot-dashed line, see the text). Plot (c) shows the concentration dependence of the diffusivities of the different species.

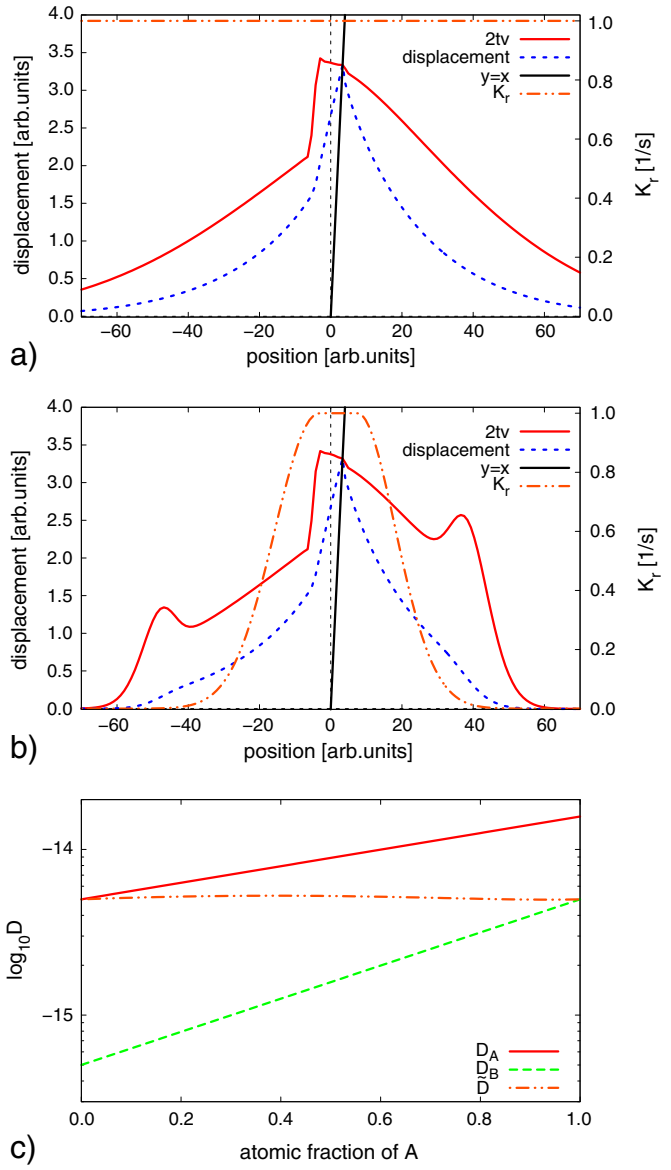


**Fig. 3.** In case of a solid solution with a miscibility gap, plot (a) shows the displacement (dashed line) as well as the velocity curve (solid red line) when the vacancy sources and sinks are evenly active at every slab. In plot (b) the same is presented but with a Gaussian vacancy source and sink distribution (dot-dashed line). Plot (c) shows the concentration dependence of the diffusivities of the different species.

(foil) and in Fig. 3b the result of a calculation with a Gaussian vacancy source and sink distribution is plotted. In this system an exponential concentration dependence of the intrinsic diffusion coefficients was supposed, no other constrain was taken into consideration, moreover there is also a miscibility gap ($0.25 < N_A < 0.75$). It can be seen that the maximum of the Kirkendall velocity is situated at the Matano and not at the Kirkendall plane. On the other hand, the maximum of the displacement and the position of the Kirkendall plane coincide. The same is true if we look at Fig. 3b, where the vacancy sources and sinks have different distributions. As can be seen, in this case as well there are other local maxima of the velocity curve, indicating again that the markers are getting closer to each other in the vicinity of these peaks. This practically would mean that the markers are "attracted" by these maxima implying three weak places along the diffusion direction. The shape of the reconstructed velocity curve on Figs. 2b and 3b is due to the space dependence of $K_r$ effectiveness factor, as well as the finite size of the film.

The presented plots so far showed only stable Kirkendall planes in a sense, that those markers which, at the end of the annealing, ended up slightly ahead of the intersection point of the velocity curve and the straight line ($2tv_K = x_K$), would slow down (lower velocity) and if these markers were behind this plane, they would move faster (higher velocity). In other words, the plane located at the intersection point tends to attract inert markers in its vicinity.

According to [21,22,25], there is no reason why the maximum in the velocity curve, the maximum in the displacement curve and the Kirkendall plane should coincide. On Fig. 4a we show a plot, where this is not the case. Moreover the Kirkendall plane in this case is unstable since, following the earlier argument, the markers which are slightly ahead of the Kirkendall plane, move faster and markers slightly behind this plane will migrate slower. Fig. 4b demonstrates the composition dependence of the diffusivities.

Experimental verification of these ideas can be found in previous studies on diffusion phenomena and the Kirkendall effect in the $\beta'$-ordered AuZn phase (B2 structure) of the binary Au–Zn system [26].

From these calculations it is clear that our model gives unexpected results concerning the position of the fiducial markers used in a so-called multifoil experiment. Applying real concentration dependent diffusivities and a spatial distribution of vacancy sinks and sources, even in these simple cases, we found, that there is indeed a Kirkendall plane which, by definition, is the plane that stays at a constant composition and moves parabolically in time during the whole interdiffusion process. On the other hand, there are other places in the diffusion zone which attract markers. That place or even those places do not move parabolically in time but, as the process goes further, attract more and more particles. As a result, such a place may become a

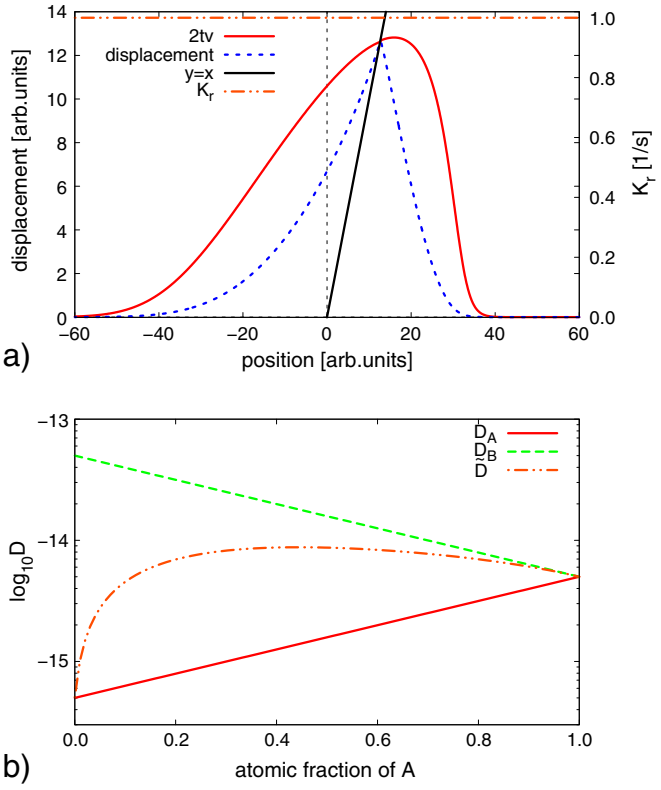


**Fig. 4.** On plot (a) the maximum of the Kirkendall velocity (solid red line) is situated at the Matano and not at the Kirkendall plane. In this calculation $K_r = 1$ in every slab. The Kirkendall plane is unstable in this case (see the text). Plot (b) shows the concentration dependence of the diffusivities of the different species.

problematic microstructural feature in any joint, because of higher mechanical failure risk at this plane.

## 4. Conclusions

Interdiffusion on the nanometer scale was investigated in the framework of our conceptual model [24]. We studied the Kirkendall shift in planar geometry in case of miscible and restrictedly miscible systems by computer simulation. A one dimensional finite volume method was developed, in which the sample was divided into $n$ slabs. The slabs mimicked the foils in the so called multifoil experiment. From the calculations we get the displacement as well as the velocity curves by registering the position of the cell walls and the number of computation cycles. Calculations were performed in two different distributions of vacancy sources and sinks i.e.: the sources and sinks are distributed evenly in the whole sample, or they followed a Gaussian distribution, having the maximum at the location of the Kirkendall plane.

It is clear that our results, concerning the position of the cell walls which act as markers in a multifoil experiment, are different from the earlier ones. Applying realistic situations, like concentration dependent diffusivities as well as spatial distribution of vacancy sinks and sources, even in very simple cases it was found that besides the Kirkendall plane there are other places in the interdiffusion specimen which attract markers. Markers placed to positions where the gradient of the velocity curve gets negative during the process get closer to each other as time goes on, resulting another condensation of the markers, which is different from the Kirkendall plane. That place, or even those places do not move parabolically in time but, as the process goes further, attract more and more particles, getting weaker and weaker in mechanical point of view.

## Acknowledgement

This work was supported by the OTKA Board of Hungary (No. NF101329), by the TAMOP 4.2.2.A-11/1/KONV- 2012–0036 and TAMOP-4.2.2/B-10/1-2010-0024 projects (implemented through the New Hungary Development Plan co-financed by the European Social Fund, and the European Regional Development Fund). The authors appreciate the help of Mark van Dal providing his experimental data presented in [20,25].

## References

[1] E. Kirkendall, L. Thomassen, C. Upthegrove, Rates of diffusion of copper and zinc in alpha brass, Trans. AIME 133 (1939) 186.
[2] E.O. Kirkendall, Diffusion of zinc in alpha brass, Trans. AIME 147 (1942) 104.
[3] A.D. Smigelskas, E.O. Kirkendall, Zinc diffusion in alpha brass, Trans. AIME 171 (1947) 133.
[4] L.S. Darken, Diffusion, mobility and their interrelation through free energy in binary metallic systems, Trans. AIME 175 (1948) 184.
[5] F. Seitz, On the theory of vacancy diffusion in alloys, Phys. Rev. 74 (1948) 1513.
[6] J. Bardeen, Diffusion in binary alloys, Phys. Rev. 76 (1949) 1403.
[7] Y.A. Geguzin, M.A. Krivoglaz, Motion of Macroscopic Inclusions in Solids, Nauka, 1979. 215 (in russian).
[8] D.L. Beke, Z. Erdélyi, I.A. Szabó, Nonlinear stress effects in diffusion, Defect Diffus. Forum 264 (2007) 117.
[9] G.B. Stephenson, Deformation during interdiffusion, Acta Metall. Mater. 36 (1988) 2663.
[10] I. Daruka, I.A. Szabó, D.L. Beke, C. Cserháti, A.A. Kodentsov, F.J.J. van Loo, Diffusion-induced bending of thin sheet couples: theory and experiments in Ti–Zr system, Acta Mater. 44 (1996) 4981.
[11] A.M. Gusak, T.V. Zaporozhets, K.N. Tu, U. Gösele, Kinetic analysis of the instability of hollow nanoparticles, Philos. Mag. 85 (36) (2005) 4445.
[12] G.E. Murch, A.V. Evteev, E.V. Levtheko, I.V. Belova, Recent progress in the simulation of diffusion associated with hollow and Bi-metallic nanoparticles, Diff. Fundam. 42 (2009) 1.
[13] C. Cserháti, G. Glodán, D.L. Beke, Hollow hemisphere formation by pure Kirkendall porosity, Diff. Foundam. 1 (2014) 61.
[14] P.G. Shewmon, Diffusion in Solids, McGraw-Hill Book Company, USA, 1963.
[15] J. Philibert, Atom Movements, Diffusion and Mass Transport in Solids, Les Editions de Physique, Les Ulis, France, 1991.
[16] R.A. Swalin, Thermodynamics of Solids, John Wiley & Sons, Inc., New York, 1972.
[17] J. Svoboda, F. Fischer, P. Fratzl, Diffusion in multi-component systems with no or dense sources and sinks for vacancies, Acta Mater. 50 (2002) 1369.
[18] J. Svoboda, F. Fischer, P. Fratzl, Diffusion and creep in multi-component alloys with non-ideal sources and sinks for vacancies, Acta Mater. 54 (2006) 3043.
[19] T. Heumann, G. Walther, Der Kirklendall-Effekt in Silber-Gold-Legirungen im gesamtem Konzentrtionsbereich, Z. Metallkd. 48 (1957) 151.
[20] M.J.H. van Dal, M.C.L.P. Pleumeekers, A.A. Kodentsov, F.J.J. van Loo, Intrinsic diffusion and Kirkendall effect in Ni–Pd and Fe–Pd solid solutions, Acta Mater. 48 (2000) 385.
[21] J.F. Cornet, D. Calais, Etude de effect Kirkendall dapres les equations de Darken, J. Phys. Chem. Solids 33 (1972) 1675.
[22] J.F. Cornet, Complements a letude de leffect Kirkendall selon les equations de Darken, J. Phys. Chem. Solids 35 (1974) 1247.
[23] F.J.J. van Loo, G.F. Bastin, G.D. Rieck, Marker displacements as a result of diffusion in binary metal systems, Sci. Sinter. 11 (1979) 9.
[24] Z. Erdélyi, G. Schmitz, Reactive diffusion and stress in spherical geometry, Acta Mater. 60 (2012) 1807.
[25] M.J.H. van Dal, Microstructural Stability of the Kirkendall Plane, Technische Universiteit Eindhoven, Eindhoven, 2001. (phd thesis edn).
[26] M.J.H. van Dal, A.M. Gusak, C. Cserháti, A.A. Kodentsov, F.J.J. van Loo, Spatio-temporal instabilities of the Kirkendall marker planes during interdiffusion in β'-AuZn, Philos. Mag. A 82 (5) (2002) 943.
[27] J. Boisse, H. Zapolsky, A.G. Khachaturyan, Atomic-scale modeling of nanostructure formation in Fe-Ga alloys with giant magnetostriction: Cascade-ordering and decomposition, Acta Materiala 59 (2011) 2656–2668.